Stretch-blow molding of PET copolymers - Influence of molecular architecture

Elise Deloye, Jean-Marc Haudin, Noëlle Billon

Stretch-Blow Molding of PET Copolymers

Influence of Molecular Architecture

E. Déloye, J.-M. Haudin*, N. Billon

MINES ParisTech, Centre de Mise en Forme des Matériaux, Sophia Antipolis, France

RUNNING TITLE: Stretch-Blow Molding of PET Copolymers

*Mail Adress : J.-M. Haudin, MINES ParisTech, Centre de Mise en Forme des Matériaux, UMR CNRS n° 7635, BP 207, 06904 Sophia Antipolis Cedex, France
E-mail : Jean-Marc.Haudin@mines-paristech.fr

Abstract

The purpose of the paper is to study the influence of molecular architecture of poly(ethylene terephthalate) (PET) on its ability to be processed by stretch-blow molding, which is not well documented in the literature. To evaluate this process ability, it proposes an original strategy combining laboratory analyses and experiments on a prototype machine.

PET copolymers were prepared from three types of comonomers: diethylene glycol (DEG), isophthalic acid (IPA) and trimethylolpropane (TMP). It is first shown, through laboratory experiments, that the nature of the polymer in terms of chain constitution (copolymerization), chain length (intrinsic viscosity) and purity (catalytic residues) greatly affects many properties: melt crystallization, thermal properties, polymer rigidity and drawability.

These different properties obviously induce very different behaviours at the different steps of the stretch-blow molding process: injection-molding of the preform (quenchability), heating (IR absorption), stretch-blow (rigidity and drawability). The stretch-blow step has been simulated on a prototype apparatus designed in our laboratory. It has been shown that free blowing can be used to characterize the process ability of the polymer. A statistical analysis has confirmed the great differences between the materials investigated and pointed out the complexity of the material response during blowing.

Keywords: stretch-blow molding, PET, molecular architecture, instrumented prototype, processing parameters, statistical analysis

1 Introduction

Stretch-blow molding is a process that allows the forming of hollow parts such as bottles. In a first step a preform is injection molded. This latter is stored and later re-heated above the glass transition temperature of the material, placed into a mold where forming takes place. The forming itself generally results from three stages: the preform is first stretched with a rod (low-blow delay), and then inflated by air at low pressure (pre-blow at 0.5 to 0.9 MPa) whilst stretching goes on. Finally, stretching is stopped and pressure is increased up to 40 bars (4 MPa). The two first stages define the so-called low-blow period whereas the last one is the blowing period. The "three-stage" distinction is not always true in industrial context: pre-blow often overlaps with stretching to prevent the touching of the preform with the stretching rod.

As far as bottles are concerned and beside specific properties required for the liquid that will fill the bottle, the converter has to guaranty the transparency, the lightness, the thickness distribution and the mechanical performances of the container. Poly(ethylene terephthalate) (PET) is one of the most appropriate materials for this application. For this polymer the above-mentioned constraints imply that the preform must be molded and blown in the amorphous state. Material must exhibit strain-induced crystallization during blowing while keeping high drawability as thickness reduction (ratio of the initial thickness of the preform to the final thickness of the bottle) can reach values from 8 to 12 during forming.

Microstructure development in PET has been extensively studied, for various types of mechanical loading, combining different techniques such as infrared, Raman and fluorescence spectroscopies, X-ray diffraction, birefringence and density measurements. An exhaustive list of relevant papers should be too long and beyond the scope of the present paper. A critical review of papers published before 2001 can be found in Gorlier et al. (2001a). Afterwards, interesting contributions have been published by Marco et al. (2002a, 2002b), Chaari et al. (2003), Mahendrasingam et al. (2003), Hsiao and co-workers (Ran et al., 2002; Kawakami et al., 2003, 2004). A key result of recent work is the probable appearance of an ordered but not well-organized phase, sometimes described as a mesophase, under strain. True crystallization would occur after deformation, in relationship with a relaxation phenomenon.

Relatively few papers have been dedicated to stretch-blow molding. A number of them have been concerned by structure development. In one of the first studies in the field, Cakmak et al.

(1984) have quantified orientation in PET bottles, and shown considerable differences between the birefringence of the inner and outer surfaces. Heterogeneity of chain orientation in the thickness was confirmed by further works (Cole et al., 1997; Gorlier, 2001; Everall et al., 2002), which led to the concept of multilayered material. To understand a complex process like stretch-blow molding, prototype machines were developed in the past (Cakmak et al., 1985; Haessley and Ryan, 1993; Kaneta et al., 1994; Schmidt 1995; Rodriguez-Villa, 1997; Wang et al., 2000). Unfortunately, the information given by such devices was insufficient, for different reasons: (i) they were not totally representative of stretch-blow molding (Rodriguez-Villa, 1997); (ii) they gave an indirect or incomplete description of polymer deformation by using an instrumented mold (Cakmak et al., 1985; Haessley and Ryan, 1993; Schmidt, 1995) or a mold with a window (Kaneta et al., 1994), respectively; (iii) even when transparent molds were used (Haessley and Ryan, 1993; Wang et al., 2000), instrumentation was not complete or heating was not representative of actual process. From this analysis, Gorlier and co-workers (Gorlier, 2001; Gorlier et al., 2001b) have designed an original prototype apparatus in order to observe the bottle formation during the low-blow period. It allowed them to follow the variations of the relevant geometrical and mechanical quantities. Such measurements have been extended to industrial line thanks to portable measuring devices (displacement, pressure and force sensors) (Salomeia, et al., 2007). Gorlier's prototype apparatus has also been used to characterize structure development in the bottles (Gorlier, 2001; Déloye, 2006; Picard and Billon, 2007; Picard, 2008).

Basically, PET results from the condensation of terephthalic acid and ethylene glycol to form a linear polyester. However, comonomers can be added to a certain amount to modify the skeleton of the molecule making it less regular, more or less rigid, or promoting short branching. Additionally, molar masses can be different from one PET to another. In consequence, different types of PET resins are available. At an industrial level it is well known that these differences can induce variable process abilities. Consequently, one key question is to understand the correlation between the chemical architecture and the behaviour of the material close to processing conditions. The general purpose of this study is then to establish such relationships for PET or, at least, to build a general strategy for estimating process ability of PET resins. Our approach is based on the combination of laboratory analyses and experiments on a prototype machine.

2 Experimental

2.1 Materials

Beside ethylene glycol and terephthalic acid, PET copolymers were prepared from three types of comonomers: diethylene glycol (DEG), isophthalic acid (IPA) and trimethylolpropane (TMP). DEG spontaneously forms during the synthesis of PET and its concentration can be partly controlled. It slows down crystallization kinetics and decreases chain stiffness. IPA is known to delay crystallization. TMP introduces some branching. The different copolymers used in this work were supplied by Tergal Fibres (Gauchy, France). They are listed in Table 1, with some of their characteristics subsequent to synthesis: viscosity index (VI) and intrinsic viscosity (IV), concentrations in antimony (Sb), acetaldehyde (AA) and terminal acid groups (TAG). Viscosity index determined according to ISO 1665/5 and DIN 53 728 norms is currently used in PET industry. To allow comparisons with literature data, intrinsic viscosities are also given. The presence of antimony is due to catalyst residues. The amounts of AA and TAG can be used as indicators of the degree of polymer degradation.

From industrial practice, the following comments can be added to Table 1. A difference of 50 units in viscosity index is significant. It is not the case for a difference of 0.2 % mol. in DEG content. Therefore, it can be stated that F9+ and F9++ differ only by chain length. Conversely, the influence of AIP content can be valuably estimated by comparing F10ssAI, AI0.6 and F10.

For processing, sufficient quantities of matter are necessary. Therefore, only commercial resins were selected. This led to some compromises, which did not allow us to vary some parameters independently of the others. This is reflected by a statistical analysis, which classifies the polymers into five groups: (i) F1CC+, PC92 and PC103; (ii) F10ssAI and AI0.6; (iii) F10, F9 and F9+; (iv) TMP; (v) F1CC. This analysis is based on the numerical values of the parameters listed in Table 1, except intrinsic viscosity (IV), since it gives the same information as viscosity index (VI). It does not take into account non-quantified parameters, which may introduce other differences between the resins.

2.2 Processing

2.2.1 Preforms and Disks

Preforms for 26 g bottles were supplied by Husky Injection Molding Systems Ltd. (Dudelange, Luxembourg). Their geometry is shown in Fig. 1. They were injection-molded according to the state of the art in order to fulfill the following requirements: (i) correct dimensions and weight; (ii) limited polymer degradation; (iii) amorphous state, proven by transparency; (iv) no residual stresses. To obtain a constant initial state for our experiments, the injection conditions were kept identical for all the formulations, except for the injection temperature, which was adjusted in the 270-280 °C range as a function of polymer viscosity. The mold temperature was 7-8 °C, to quench the polymer into the amorphous state. 2mm-thick disks were also injection-molded by Rhodia (Saint-Fons, France) in analogous conditions. The transparency of the specimens was checked by visual observation. The viscosity indices as well as the AA and TGA contents were measured after injection. They indicated a limited degradation, the main feature being an increase of AA concentration, particularly in preforms.

2.2.2 Bottles

Bottles were manufactured on a prototype apparatus designed in our laboratory (Gorlier, 2001; Gorlier et al., 2001b). It aims at being as representative of the process and as instrumented as possible. However, as a first step, only the low-blow period is considered. The preforms are heated in an infrared oven consisting of five independently-controlled lamps, which produces appropriate temperature gradients in the preforms. The preform neck is maintained at room temperature and used to transfer the preform from the oven to the stretch-blow set-up. Any sequence of stretching and pre-blowing can be imposed. The stretching velocity can reach 800 mm/s and the stretching distance can be varied up to 170 mm. Low-blow delay can be controlled as well as pressure and duration of pre-blow. The quenching effect of the mold is reproduced by air jets allowing a homogeneous cooling of the external surface of the bottle. They enable a cooling rate of about 600 °C/min and a freezing of the blown geometry. Obviously, neither the final blowing phase, nor the interaction of the material with the mold can be reproduced, as the prototype machine has no mold. This prototype apparatus is well adapted to the present work, since we want to characterize the intrinsic deformability of the resins as a function of their molecular architecture, without the geometrical constraints imposed by the mold.

The stretching force and displacement, the pressure in the blowing nozzle and inside the preform are measured as a function of time in addition to the initial temperature of the PET (using a dot IR pyrometer). The different steps of the forming of the bottle can be observed with a high sampling rate video camera and connected to the macroscopic parameters recorded. Specific marked preforms make it possible to measure local strain and strain rate as a function of time.

In the present work, the prototype apparatus was used in two distinct ways. In a first step, the influence of processing parameters was statistically analyzed in a classical configuration, i.e., with a stretching rod (See Section 4.2). Then, taking into account the results of this first analysis, in-depth investigation of the process ability of the resins was carried out in a situation of free blowing, i.e., without stretching rod (See Section 4.3).

2.3 Thermal Measurements

To master the heating process in the oven, IR absorption of the different amorphous PET was studied at the Ecole des Mines d'Albi-Carmaux (France). Measurements were done in transmission in the 1-2.2 μm wavelength range using a Fourier transform infrared spectrometer (Spectrum 2000, PerkinElmer). The specimens were injected plates with a thickness ranging from 2.5 to 3.5 mm. They made it possible to calculate an average absorption coefficient and a penetration depth, which is the reciprocal of this coefficient.

2.4 Calorimetry

Polymer crystallization and melting were investigated by Differential Scanning Calorimetry (DSC-7, PerkinElmer). The calorimeter was calibrated in temperature and energy with indium and tin. The specimens were cut off from 250 μm-thick films prepared by melting pellets on a hot stage between two glass slides coated with polytetrafluorethylene. Prior to melting the pellets were dried 15 h at 130 °C under vacuum. The DSC protocol was the following: (i) heating at 10 °C/min and then 5 min holding at 290 °C, (ii) cooling down to 20 °C at a constant rate in the 5-30 °C/min range, and (iii) finally heating at 10°C/min up to 290 °C.

2.5 Viscoelastic Measurements

The linear viscoelastic properties were characterized by Dynamical Mechanical Analysis (Tritec 2000 DMA, Bohlin Instruments). The apparatus was operated in the single cantilever deformation mode with an imposed displacement of 5 μm to remain in the linear domain. Parallelepiped-shaped specimens were machined along the flow direction from performs and disks, with the following dimensions: $5 \times 3 \times 2$ mm^3 (preforms) and $5 \times 2 \times 1$ mm^3 (disks).

For the samples machined from the preforms, analyses were carried out between 0.316 and 31.6 Hz at a heating rate of 1 °C/min. The aim was to determine the processing temperature range. The specimens coming from the disks were analyzed in isothermal experiments performed every five degrees between 75 and 100 °C, frequency being varied between 0.1 and 100 Hz. The results were used to plot master curves thanks to time-temperature equivalence.

2.6 Tensile Testing

The large-strain behaviour was investigated on flat hourglass-shaped specimens with a thickness of 2 mm. Shape was chosen such as necking was initiated in the central zone, where marks were put to allow video extensometer measurements (Fig. 2). Samples were machined out of the injected disks, systematically perpendicular to the flow direction though no evidence for mechanical anisotropy could be observed. Seven dots were printed on the specimen surface and the deformation was followed by a high sampling rate video camera, which made it possible to determine longitudinal and transverse strains (G□sell et al., 2002). In this paper, as materials were close to be incompressible, only the five vertical dots were taken into account. The true axial strain and stress are given by:

$$\varepsilon = \ln \frac{l}{l_0} \text{ and } \sigma = \frac{F}{S_0} \exp \varepsilon \qquad (1)$$

l and l_0 are the current and initial lengths between two dots, F is the load and S_0 the initial section. The value of ε used to calculate the stress is obtained by interpolation of the strains calculated between two successive dots.

Tensile experiments were performed using a hydraulic Instron 1341 machine at 80, 85 and 95 °C for different crosshead velocities: 0.5, 10 and 150 mm/s. As in previous work (Gorlier

et al., 2001a), cooled clamping devices were used together with a specific protocol consisting in cooling the shoulders as late as possible to keep the temperature of the central zone of the specimen constant during the entire test without deforming these shoulders.

3 Results and Discussion: Polymer Characterization

3.1 Crystallinity

To evaluate the crystallization ability of all copolymers, two parameters were selected: (i) the crystallization temperature T_c, taken at the maximum of the DSC peak, with an estimated uncertainty of ± 1 °C; (ii) the mass crystallinity ratio X_c, deduced from the area of the crystallization peak, with an absolute error ranging from ± 3 % ($X_c \sim 40\,\%$) to ± 1 % ($X_c \sim 10\,\%$). The theoretical enthalpy of fusion was taken equal to 120 J/g (Wunderlich, 1980).

For all the copolymers, crystallization temperature decreases with increasing cooling rate (Fig. 3). However, significant differences, i.e., greater than the experimental error, and up to about 20 °C, are observed between some resins: for instance, F10ssAI exhibits the highest T_c and PC103 the lowest. Crystallinity also decreases with cooling rate (Fig. 4), with important differences between some resins. By extrapolation to zero crystallinity, it is possible to deduce a critical cooling rate, which has to be reached to quench PET into the amorphous state. This critical value ranges between 36 °C/min (PC103) and 150 °C/min (F10ssAI). The upper limit is close to some data of the literature (Brucato et al., 1995) but still lower than others (300 °C/min) (Baltá Calleja et al., 2000), illustrating the wide variation range of hot crystallisation for PET resins.

Our first conclusion is that chain architecture can significantly influence quiescent crystallization kinetics. For instance, the presence of IPA (comparison between F10ssAI and F10) and an increase in viscosity (comparison of PC92 and PC103) help quenching into amorphous state. However, if crystallinity is plotted against crystallization temperature (Fig. 5), a kind of master curve is obtained for linear PET. Different results are obtained for TMP due to branching. Consequently, for linear PET, chemical modifications of the chain do not seem to modify the intrinsic crystallization phenomena, and the differences observed could be

due to kinetic effects in terms of nucleation and growth. Nucleation is very sensitive to synthesis conditions, especially to the amount of catalyst residues (Sb). The spherulite growth rate is affected by chain regularity (e.g., presence of IPA) and molecular mobility in the melt (e.g., influence of molar mass). A more detailed analysis can be found in (Déloye, 2006; Déloye et al., 2008). Nevertheless, despite a good characterization of the resins, it is difficult to draw straightforward correlations between molecular parameters and quiescent crystallization phenomena. A great scatter of the overall kinetics data concerning PET has been reported in the literature. For instance, Hieber (1995) has compared bibliographic data concerning PET isothermal crystallization, and shown that for all the resins under consideration, the fastest crystallization occurred at about the same temperature (172 °C), but with quite different half-crystallization times (from 5 to 500 s). The influence of molar mass and catalyst residues has also been mentioned.

From a practical point of view, these results are very important since they give information on the quenching ability of thick preforms. For instance, for F10ssAI which crystallizes faster, some opalescence due to crystallization could be observed in the preforms though they were still acceptable for blowing.

3.2 Thermal Properties

Fig. 6 shows the variation of the penetration depth as a function of the source temperature. In all cases, an increase in the heating power logically leads to a longer path for the wave inside the material. Chemical modifications induce different thermal behaviours. Introduction of IPA favours heat propagation, especially at high temperature, as shown by the comparison between F10ssAI and F10. TMP exhibits the highest absorption. The role of DEG is less clear. For instance, the behaviours of F1CC and F1CC+, which have different compositions, are quite similar. On the contrary, this similarity is not observed for F9+ and F9++, which have almost the same composition. Moreover, catalyst residues (Sb particles) may play a role on absorption.

As a result of these different thermal properties, identical technological heating conditions lead to significantly different temperatures in different resins (a difference up to 15 degrees in our case). This should induce important artefacts in the characterization of PET process ability. This is of high importance and should be addressed in any study of polymer

processing when infrared technology is involved. In the present study the heating power was adjusted, for all the resins, to study the process at a given and known temperature at the external surface. This was experimentally calibrated and adjustment concerned only the general power delivered to the oven. Polymers with a low penetration depth, e.g. TMP and F10ssAI, were then more intensively heated at the surface and consequently, for these polymers the power of the oven had to be reduced.

Furthermore, it has been checked elsewhere (Déloye, 2006) that for a given initial temperature of the outer surface, the temperature gradient in the preform thickness does not depend on the formulation. This validates our protocol for controlling temperature in the different resins by controlling the external temperature of the preform.

3.3 Viscoelastic Properties

Typical DMA curves recorded for two different frequencies are displayed in Fig. 7. The main features for the elastic modulus E' are: a sharp drop at the α transition, a rubber plateau interrupted at about 113 °C because of cold crystallization which increases polymer stiffness. The frequency dependence is clearly shown: the α transition temperature, T_α, taken at the maximum of the tangent of loss angle, is shifted by 8 °C towards higher temperatures when the frequency is multiplied by 100. Conversely, the cold crystallization temperature is quasi independent of frequency. Such results make it possible to determine the processing temperature range as a function of frequency, i.e. of strain rate. This range is limited by the α transition temperature on one hand, and the cold crystallization temperature on the other hand (Fig. 8). It can be observed that the processing range becomes narrower when strain rate increases. This of practical importance, since strain rates can reach 100 s^{-1} in the process. All the formulations exhibit similar stain-rate sensitivities, but differences in molecular mobility are observed. Increase of molar mass shifts T_α towards higher temperatures (comparison of F9+ and F9). IPA also increases T_α (comparison of F10 and F10ssAI). TMP shows a lower T_α, which is not so easy to explain, since this polymer is branched but also contains more DEG. Finally, as the industrial processing range is usually 90-110 °C, all the polymers exhibit a rubber-like behaviour in this interval, but with a non-negligible viscous component.

This first approach was completed by the analysis of master curves obtained with five representative polymers at the reference temperature of 90 °C (Fig. 9). The curves for F10ssAI, F9 and TMP are relatively close to each other. Those for PC 103 and F1CC+ are quite different with a higher plateau modulus. This shows the predominant effect of chain length, which has been confirmed on other formulations (Déloye, 2006). Other chemical parameters (% IPA, % DEG, branching) do not seem to have a significant influence. As suggested above, some compensation between the respective effects of branching and DEG content might occur in TMP.

3.4 Large-Strain Behaviour

First of all, the master curves established by DMA were used to transform the experimental conditions (temperature, crosshead velocity) into values of strain rate at the reference temperature $T_{ref} = 90\,°C$ (Table 2). This enabled us to plot true stress vs. true strain curves at T_{ref} for different strain rates (Fig. 10). These curves exhibit strain hardening attributed to ordered entities, which do not constitute a fully developed crystalline phase (Gorlier et al., 2001a). The onset of strain hardening can be characterized by a stress σ_{DR} and a strain ε_{DR} determined as indicated in Fig. 10. ε_{DR} corresponds to the so-called natural draw ratio. Fig. 11 shows the variations of σ_{DR} and ε_{DR} with strain rate. In agreement with previous results, PC 103 and F1CC+ are less easily deformed (higher σ_{DR} stresses, Fig. 11A). Fig. 11B clearly shows the two families of copolymers identified in Fig. 9. For all of them, the ε_{DR} variation is not monotonic. A minimum is observed depending on the family: at about 0.1 s^{-1} for PC 103 and F1CC+, and at about 10 s^{-1} for F10ssAI, F9 and TMP. It cannot be attributed to self-heating, because it should also have an effect on σ_{DR}. The hypothesis of another deformation mechanism can be put forward, since at high strain rate the rubber plateau has been left and the polymer can partially exhibit glassy processes.

4 Results and Discussion: Processing

4.1 The Notion of "Good Bottle"

First experiments were done with the copolymer F9, which is a standard grade. The objective was to define operating conditions leading, more or less subjectively, to a "good bottle" fulfilling the following conditions: (i) a volume close to the volume of the actual bottle

associated with the preform; (ii) a shape as close as possible to the ideal geometrical representation given in Fig. 12, i.e., a cylindrical body and well-rounded extremities; (iii) thickness regularity; (iv) transparency, appreciated by visual observation. Fig. 12 shows a photograph of such a "good bottle". The appropriate processing conditions are gathered in Table 3. For heating, six parameters have to be considered: the powers of the five independent lamps, given as percentages of a maximum power, and the total power of the oven, also expressed as a fraction of the maximum power. Temperature is measured on the external surface at two centimetres below the neck. After these adjustments, only the total power of the oven was varied to control the preform temperature (see Section 3.2).

4.2 Influence of Processing Parameters

In a second step, the relative importance of relevant processing parameters was estimated using a complete factorial plan (Vigier, 1988). These parameters are listed in Table 4 with the values retained for the experiments. A bottle was described by four parameters: its total volume including the neck, its maximum diameter and total length, and a shape factor equal to the ratio of the measured volume to a theoretical one, the bottle being modelled by two half-spheres connected by a cylinder (Fig. 12). The statistical analysis of the experiments was performed with the software StatGraphics® Plus Version 5.1. The results can be visualized in the form of Pareto's diagrams (Fig. 13), which quantify the importance of each parameter as well as their crossed influences (e.g., AB).

The statistical analysis shows that low-blow delay (E) has little effect on the final bottle in the present study (it may be important in production machines to prevent the stretched preform from touching the stretch rod). On the contrary, low-blow duration (C) has the most important influence, from a technical point of view. Unfortunately, the industrial objective is to reduce the cycle time. Therefore, we were obliged to renounce this parameter. Temperature and pressure are important parameters, either isolated (A and B), or in combination (AB), which can be related to time-temperature equivalence. As a consequence of this relationship, only temperature was varied. Finally, the role the stretching rod (D) seems not very significant. This could be due to the short rod lengths used here.

4.3 Experimental Analysis of Free Blowing

As the role of the stretching rod is not very important in the present work, the study was continued without stretching rod, i.e., in a situation of free blowing. After preliminary experiments (Déloye, 2006), it was restricted to the five typical copolymers already considered above: F9, F10ssAI, TMP, PC 103 and F1CC+. Pressure and low-blow duration were left at their standards values given in Table 3. One has to keep in mind that even if blowing pressure is kept constant, actual pressure inside the preform varies during time. Fig. 14 shows the video recording of a typical experiment. For all the bottles, a bubble is initiated under the neck. Pressure increases during the very first stage, passes through a maximum when this bubble reaches its final diameter, and decreases as an image of the subsequent increase in volume. This maximum pressure obviously depends on blowing conditions that are imposed but also, to a large extent, on temperature, on preform thickness and on the resin itself. This kinematics also creates a pronounced shoulder at the upper zone of each bottle. Conversely, the bottom of the bottle greatly depends on blowing conditions. An overthickness is observed in some cases due to undeformed matter.

Temperature was varied between 80 and 120 °C, but only bottles with a good transparency and without optical defects were kept for further analysis. They correspond to a temperature range where the polymer is rubber-like, in agreement with viscoelastic measurements (see Fig. 8).

Fig. 15 shows the variations of the bottle volume with temperature. Some correlations can be established with viscoelastic properties and especially with the plateau modulus, which characterizes the stiffness of the material (see Fig. 9). In both cases, two groups can be distinguished. Logically, the stiffest resins (PC 103 and F1CC+) give the smallest bottles and the greatest volume is obtained with the softest polymer (TMP). Nevertheless, F10ssAI and F9, which are close in terms of rigidity, lead to significantly different bottle volumes.

Local extension can be measured as a function of time by following the deformation of a mesh graven on the external surface of the preform (Fig. 14). This was done for an element near the neck, because in this region the material is fully deformed. Fig. 16 gives a typical example of the time dependence of transverse extension, together with its time derivative, strain rate, which passes through a maximum. This maximum, averaged over longitudinal and transverse directions, can be taken as a characteristic of the process. As a consequence of time-temperature equivalence, bottle volume can be plotted as a function of this strain rate

$\dot{\varepsilon}_{\max,av}$ at $T_{ref} = 90\,°C$ (Fig. 17). The global trends are confirmed, but the specificity of TMP is enhanced. It also appears that each copolymer "naturally" imposes its own strain-rate range.

Fig. 18 shows the time evolutions of the longitudinal and transverse extensions for the PET F9 at 100 °C. Remarkably, the longitudinal deformation exhibits a delay with respect to the transverse one. This occurs during the first stages of blowing when the preform size globally increases under the effect of pressure (see Fig. 14). Then, after some critical strain the bubble is initiated. This phenomenon, which was observed for all the polymers, was characterized by a parameter $\lambda_{L/T}$ equal to the ratio of the times corresponding to an arbitrary extension of 1.1. This parameter will be used in the following statistical analysis. As a consequence of this delay, the longitudinal extension is always lower than the transverse one.

4.4 Statistical Analysis of Free Blowing

For a more complete understanding of the blowing process, a statistical analysis was performed with the softwares StatGraphics® Plus and Uniwin. Version 5.1 The PCA technique (principal component analysis) (Bialès, 1988; Giannelloni and Vernette, 1995) was used. In the PCA technique, initial standardized variables are transformed into new ones, called "principal components", by linear combinations.

The general idea was that process ability should be driven by the initial rigidity of the material and by the strain hardening process, together with their dependences upon strain rate and temperature. Statistical analysis was hoped to draw some relationships between material properties (as measured here) and process ability, referred to as the ability to form the arbitrarily defined good bootle.

In a first attempt, five initial variables were selected. Some of them were assumed to represent processing conditions while others were supposed to be material characteristics. The technological ones were surface temperature of the preform (*T*), maximum pressure during blowing ($P_{\max}$) and averaged maximum strain rate ($\dot{\varepsilon}_{\max,av}$) during blowing. The material parameters were the values of the stress and the strain at the onset of strain hardening during tensile tests at a strain rate of $\dot{\varepsilon}_{\max,av}$ ($\sigma_{DR,\dot{\varepsilon}_{\max}}$ and $\varepsilon_{DR,\dot{\varepsilon}_{\max}}$), i.e., in conditions close to process conditions. Two components were retained. Their inertias (fraction of information

contained in initial variables) are 69.3 % and 19.3 %, respectively. The results, in terms of bottle volume, are displayed in Fig. 19. The axes correspond to the initial variables. Points located near a given axis and far enough from the origin imply a strong influence, positive or negative, of the corresponding parameter. On the contrary, orthogonality means independence of this parameter. The diagram of Fig. 19 makes it possible to clearly identify the different categories of bottles. As an example, the region of "underblown bottles" is along the $\dot{\varepsilon}_{\max,av}$, $\sigma_{DR,\dot{\varepsilon}_{\max}}$ and T axes. This means that the volumes were limited because of a too low temperature and likely a lack of molecular mobility. "Good bottles" result from a subtle equilibrium between the effects of all the parameters. The relative positions of the "good bottles" and "slightly overblown bottles" regions show that a temperature increase leads to a volume excess. Finally, the region of "overblown bottles" is mainly confined between the T and $\varepsilon_{DR,\dot{\varepsilon}_{\max}}$ axes.

In a second analysis, six material characteristics were chosen: (i) the average preform temperature (T_{av}); (ii) the elastic modulus (E') at T_{av}, which characterizes material stiffness; (iii) the shift factor (a_T) used for the time-temperature equivalence, which contains rate effects; (iv) the parameter $\lambda_{L/T}$ introduced above, to account for unbalanced biaxial deformation; (v) $\dot{\varepsilon}_{\max,av}$; (vi) $\sigma_{DR,\dot{\varepsilon}_{\max}}$. Fig. 20 illustrates the complexity of the material response during blowing. It is difficult to propose simple correlations between blowing kinematics and material characteristics. Nevertheless, temperature sensitivity of the chain and its stiffness seem to determine, at least partly, the onset of the bubbles. In the same way, temperature and polymer deformability are favourable to bubble development.

The statistical analysis underlines the differences between materials. PC 103 and F1CC+ always give good or quasi acceptable bottles. Conversely, F10ssAI, F9, PC 103 have no intermediate stage between under-and overblowing. This shows that the processing window is proper to each formulation.

5 Conclusion

The present work has shown that the nature of the polymer in terms of chain constitution (copolymerization), chain length (intrinsic viscosity) and purity (catalyst residues) greatly

affects many aspects of PET behaviour: melt crystallization, thermal properties, polymer rigidity and drawability. Although the final crystallinity seems to be controlled by thermodynamic considerations, the crystallization kinetics considerably varies from a polymer to another. It has been discussed in terms of nucleation and growth. Nucleation seems to be sensitive to the amount of catalyst residues. The spherulite growth rate may be affected by chain regularity which is disturbed by random copolymerization and molecular mobility in the melt which is related to the influence of molar mass (Déloye, 2006; Déloye et al., 2008). IR absorption also depends on the chain structure and/or residues. As a practical consequence, the heating power must be adjusted for each resin to obtain a prescribed surface temperature, when infrared technology is used. Concerning rigidity and drawability, only the role of chain length has been clearly identified.

These different properties obviously induce very different behaviours at the different steps of the processing chain: injection-molding of the preform (quenchability), heating (IR absorption), stretch-blow (rigidity and drawability). The stretch-blow step has been simulated on a prototype apparatus without mold, in order to follow bottle formation, except for the final contact with the mold. After a preliminary analysis, it has been shown that free blowing was able to account for the process ability of the polymer. A statistical analysis has confirmed the great differences between the materials. It has pointed out the complexity of the material response during blowing. Therefore, it is difficult to propose straightforward correlations between blowing kinematics and material characteristics. The final bottle is the result of a subtle combination of several parameters. Nevertheless, both direct and statistical analyses have shown an influence of temperature. After a more detailed study, it seems more relevant to cast temperature and strain-rate effects in a unique parameter using the time-temperature equivalence.

Beyond the intrinsic complexity of the problem, a difficulty of this work was to vary one parameter of the molecular structure independently of others. For example, the effects of branching are probably masked by an important amount of DEG. To extend this work, it would be desirable to prepare tailored polymers using a pilot reactor able to produce sufficient quantities for processing. In any case, the methodology proposed here is applicable to polymers other than PET. A slight improvement could be to characterize the drawabililty in biaxial stretching.

Acknowledgements

The authors acknowledge financial support from ANVAR and Tergal Fibres, within the framework of the PROSPET program. They want to express their gratitude to G. Pérez, who was the initiator of this program. They also thank J.-L Lepage for technical help and stimulating scientific discussions.

References

Baltá Calleja, F. J., et al., "Structure development in poly(ethylene terephthalate) quenched from the melt at high cooling rates : X-ray scattering and microhardness study", Polymer, **41**, 4143-4148 (2000),
DOI:10.1016/S0032-3861(99)00640-0

Bialès, C.: L'analyse statistique des données. L'outil statistique appliqué au marketing et à la gestion, Editions Chotard et Associés, Paris (1988)

Brucato, V., et al., "Analysis of nonisothermal crystallisation kinetics of PET", Proc. Eur. Regional Meeting of the PPS, Stuttgart, Germany (1995)

Cakmak, M., et al., "A basic study of orientation in poly(ethyleneterephthalate) stretch-blow molded bottles", Polym. Eng. Sci., **24**, 1390-1395 (1984).
DOI:10.1002/pen.760241804

Cakmak, M., et al., "An investigation of the kinematics of stretch blow molding of poly(ethylene terephthalate) bottles", J. Appl. Polym. Sci., **30**, 3679-3695 (1985),
DOI:10.1002/app.1985.070300913

Chaari, F., et al., "Crystallization of poly(ethylene terephthalate) under tensile strain: crystalline development versus mechanical behaviour", Polymer 44, 473-479 (2003),
DOI:10.1016/S0032-3861(02)00739-5

Cole, K. C., et al., "Orientation and conformation in PET: new information from specular reflection FT-IR", Mikrochim. Acta Suppl., **14**, 403-405 (1997)

Déloye, E.: Effet de l'architecture de chaîne sur le comportement en injection soufflage de copolyesters PET -étude expérimentale-, PhD Thesis, Ecole Nationale Supérieure des Mines de Paris, Sophia Antipolis (2006)

Déloye, E., et al., "Influence of chemical architecture of PET on ability to stretch blow moulding", Int. J. Material Forming, **1**, Supplement 1, 715-718 (2008),
DOI: 10.1007/s12289-008-0315-6

Everall, N., et al., "Characterization of biaxial orientation gradients in poly(ethylene terephthalate) films and bottles using polarised attenuated total reflection FTIR spectroscopy", Polymer, **43**, 4217-4223 (2002),
DOI:10.1016/S0032-3861(02)00247-1

Giannelloni, J. L., Vernette, E.: Etudes de marché, Editions Vuibert, Paris (1995)

Gorlier, E.: Caractérisation rhéologique et structurale d'un PET. Application au procédé de bi-étirage soufflage de bouteilles, PhD Thesis, Ecole Nationale Supérieure des Mines de Paris, Sophia Antipolis (2001)

Gorlier, E., et al., "Strain induced crystallisation in bulk amorphous PET under uni-axial loading", Polymer, **42**, 9541-9549 (2001),
DOI:10.1016/S0032-3861(01)00497-9

Gorlier, E., et al., "Instrumented prototype for stretch-blow moulding of PET: a tool for understanding properties-processing relationships", 4th ESAFORM Int. Conf. on Material Forming, Liège, Belgium, 345-348 (2001)

G□sell, C., et al., "Experimental characterization of deformation damage in solid polymers under tension, and its interrelation with necking", Int. J. Solids Struct., **39**, 3857-3872 (2002),
DOI:10.1016/S0020-7683(02)00184-1

Haessley, W. P., Ryan, M. E., "Experimental study and finite element analysis of the injection blow molding process", Polym. Eng. Sci., **33**, 1279-1287 (1993),
DOI: 10.1002/pen.760331908

Hieber, C. A., "Correlations for the quiescent crystallization kinetics of isotactic polypropylene and poly(ethylene terephthalate)", Polymer, **36**,1455-1467, (1995),
DOI:10.1016/0032-3861(95)95925-Q

Kawakami, D., et al., "Mechanism of Structural Formation by Uniaxial Deformation in Amorphous Poly(ethylene terephthalate) above the Glass Temperature", Macromolecules, **36**, 9275-9280 (2003),
DOI**:** 10.1021/ma034791b

Kawakami, D., et al., "Structural formation of amorphous poly(ethylene terephthalate) during uniaxial deformation above glass temperature", Polymer, **45**, 905-918 (2004),
DOI:10.1016/j.polymer.2003.11.027

Kaneta, T., et al., "Direct observation of blow moulding process from inside the parison", Proc. 10th Ann. Meeting of the PPS, Akron, USA, 294-295 (1994)

Mahendrasingam, A., et al., "Observation of structure development during crystallisation of oriented poly(ethylene terephthalate)", Polymer, **44**, 5915-5925 (2003),

DOI:10.1016/S0032-3861(03)00542-1

Marco, Y., et al., "Induced crystallization and orientation of poly(ethylene terephthalate) during uniaxial and biaxial elongation", Macromol. Symp., **185**, 15-34 (2002),
DOI: 10.1002/1521-3900(200208)185:1<15::AID-MASY15>3.0.CO;2-J

Marco, Y., et al., "WAXD study of induced crystallization and orientation in poly(ethylene terephthalate) during biaxial elongation", Polymer, **43**, 6569–6574 (2002),
DOI:10.1016/S0032-3861(02)00488-3

Picard, M.: Evolution de la microstructure d'un PET lors du bi-étirage soufflage; Corrélation au durcissement structural, PhD Thesis, Ecole Nationale Supérieure des Mines de Paris, Sophia Antipolis (2008)

Picard, M., Billon, N., "Microstructural evolution of PET under stretching and during stretch blow moulding", 10th ESAFORM Int. Conf. on Material Forming, Zaragoza, Spain (2007)

Ran, S., et al., "Mesophase as the Precursor for Strain-Induced Crystallisation in Amorphous poly(ethylene terephthalate) Film", Macromolecules, **35**,10102-10107 (2002),
DOI: 10.1021/ma021252i

Rodriguez-Villa, A.: Etude théorique et expérimentale de l'extrusion-soufflage de corps creux en polymère, PhD Thesis, Ecole Nationale Supérieure des Mines de Paris, Sophia Antipolis (1997)

Salomeia, Y., et al., "Experimental Investigation of Process Conditions of Stretch Blow Moulding", 10th ESAFORM Int. Conf. on Material Forming, Zaragoza, Spain (2007), published in AIP Conf. Proc., **907**, 896-901 (2007)

Schmidt, F.: Etude expérimentale et modélisation du procédé d'injection/soufflage bi-orientation en cycle froid de bouteilles en P.E.T., PhD Thesis, Ecole Nationale Supérieure des Mines de Paris, Sophia Antipolis (1995)

Vigier, M. G.: Pratique des plans d'expériences, Paris, les Editions d'Organisation, Paris (1988)

Wang, S., et al., "Viscoplastic Material Modeling for the Stretch Blow Molding Simulation", Int. Polym. Proc., **15**, 166-175 (2000)

Wunderlich, B.: Macromolecular Physics, Vol. 3, Crystal Melting, Academic Press, New York, 69 (1980)

Captions for the figures

Figure 1. Shape and dimensions in mm of the preform.

Figure 2. Shape and dimensions in mm of the tensile specimens. Thickness: 2 mm. Location of the seven dots printed on the specimen surface in order to follow the deformation with a video camera.

Figure 3. Crystallization temperature, taken at the maximum of the DSC peak, vs. cooling rate. Error bar: ± 1 °C.

Figure 4. Mass crystallinity, deduced from the area of the crystallization peak, vs. cooling rate. Error bars: ± 3 % for $X_c \sim 40$ % and ± 1 % for $X_c \sim 10$ %.

Figure 5. Mass crystallinity vs. crystallization temperature, deduced from the results of Figs. 3 and 4.

Figure 6. Penetration depth of IR radiation into PET copolymers vs. source temperature, which characterizes heating power.

Figure 7. DMA curves showing the temperature variations of the elastic modulus E' and of the loss tangent $\tan\delta$ at two frequencies. F10ssAI copolymer.

Figure 8. Frequency dependences of the α transition temperature (lower points, error bar: ± 0.5 °C) and the cold crystallization temperature (upper points, error bar: ± 1 °C), deduced from DMA measurements.

Figure 9. Master curves of the elastic (storage) modulus for five representative polymers at the reference temperature of 90 °C. These curves are established from DMA results using time-temperature equivalence

Figure 10. True stress vs. true strain (Hencky strain) curves as a function of strain rate at the reference temperature of 90 °C. F10ssAI copolymer. Definition of the stress σ_{DR} and the strain ε_{DR} at the onset of strain hardening. The strain rates at 90 °C are calculated from temperatures and crosshead velocities using time-temperature equivalence (see Table 2).

Figure 11. Variations of the stress σ_{DR} (A) and the strain ε_{DR} (B) at the onset of strain hardening as a function of the strain rate at $T_{ref} = 90$ °C. σ_{DR} and ε_{DR} are defined in Fig 10.

Figure 12. Photograph of a "good bottle" and ideal geometrical representation.

Figure 13. Pareto's diagrams for the geometrical characteristics of a bottle. Only the results at the right of the vertical white line are significant. Arbitrary units.

Figure 14. The different steps of bottle formation in a free-blowing configuration. Observations of the deformation of a mesh graven on the external surface of the preform.

Figure 15. Bottle volume vs. preform temperature in a free-blowing configuration for five representative copolymers.

Figure 16. Time evolutions of the transverse extension and strain rate deduced from the video recording of the deformation of a mesh element located near the neck. The mesh graven on the external surface of the preform can be seen shown in Fig. 14. Copolymer F9 at 102.8 °C.

Figure 17. Bottle volume vs. $\dot{\varepsilon}_{\max,av}$ at $T_{ref} = 90\,°C$ for five representative copolymers. This characteristic strain rate is calculated, using time-temperature equivalence, from the average of the maximum longitudinal and transverse strain rates reached during the deformation of a mesh element (see Fig. 16).

Figure 18. Time evolutions of local longitudinal and transverse extensions for PET F9 at 100 °C, deduced from the deformation of a mesh element.

Figure 19. First principal component analysis from technological (*T*: surface temperature of the preform; $P_{\max}$: maximum pressure during blowing; $\dot{\varepsilon}_{\max,av}$: averaged maximum strain rate during blowing) and material ($\sigma_{DR,\dot{\varepsilon}_{\max}}$ and $\varepsilon_{DR,\dot{\varepsilon}_{\max}}$: stress and strain at the onset of strain hardening for $\dot{\varepsilon}_{\max,av}$) parameters. The numbers correspond to the bottle volumes (in mL).

Figure 20. Second principal component analysis from six material characteristics: T_{av} (average preform temperature), E'(elastic modulus at T_{av}), a_T (shift factor for time-temperature equivalence), $\lambda_{L/T}$ (parameter accounting for unbalanced biaxial deformation), $\dot{\varepsilon}_{\max,av}$ (averaged maximum strain rate during blowing), $\sigma_{DR,\dot{\varepsilon}_{\max}}$ (stress at the onset of strain hardening for $\dot{\varepsilon}_{\max,av}$). The numbers correspond to the bottle volumes (in mL).

Captions for the tables

Table 1. Main characteristics of the copolymers.

Table 2. Correspondence between tensile testing parameters and strain rates in s^{-1} at the reference temperature of 90 °C.

Table 3. Standard values of the processing parameters for a "good bottle".

Table 4. Values of the processing parameters in the factorial plan.

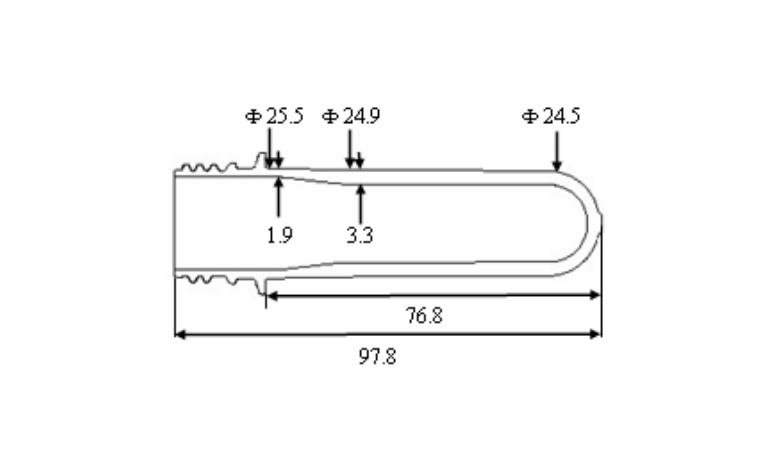

Fig. 1

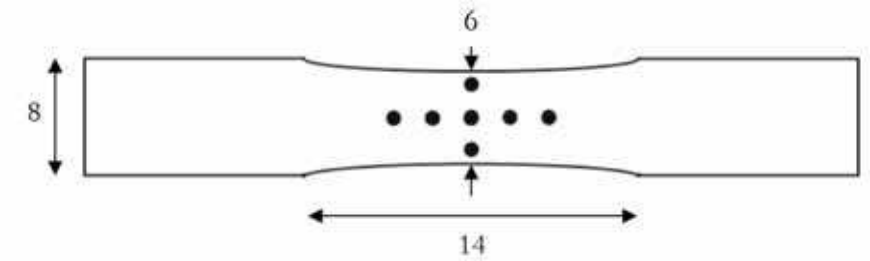

Fig. 2

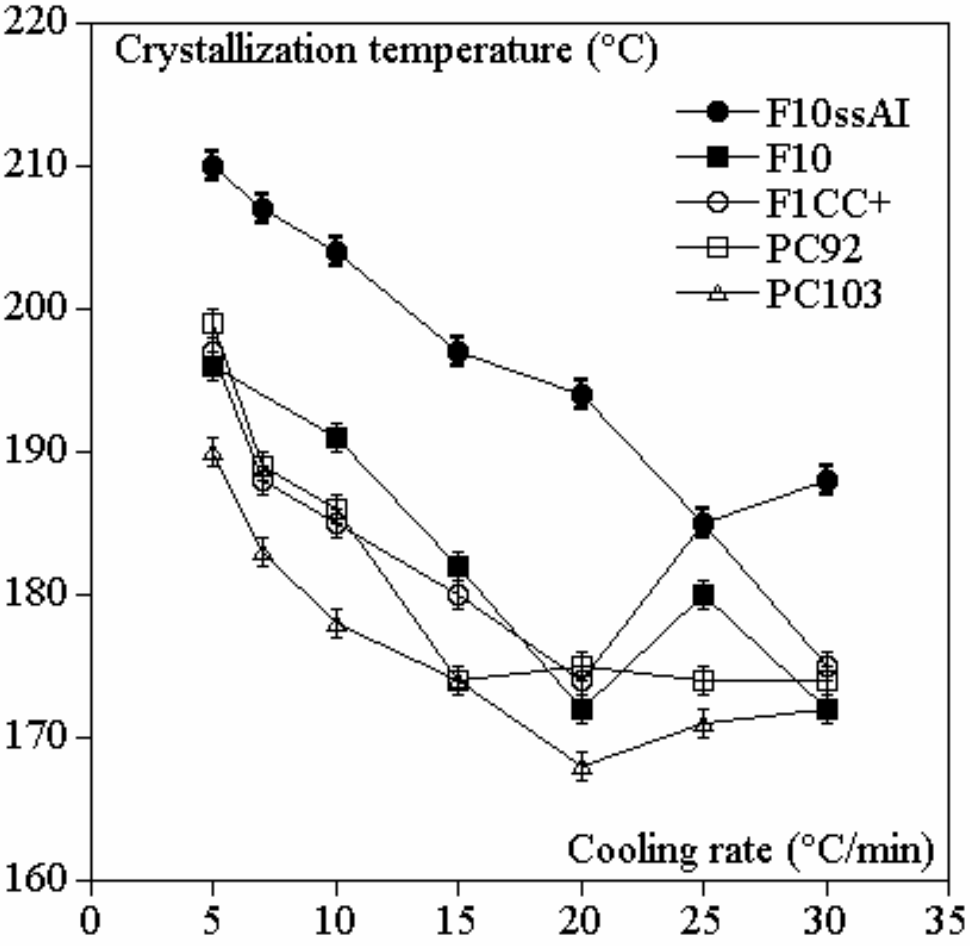
Crystallization temperature (°C)
F10ssAI
F10
F1CC+
PC92
PC103
Cooling rate (°C/min)
220
210
200
190
180
170
160
0
5
10
15
20
25
30
35

Fig. 3

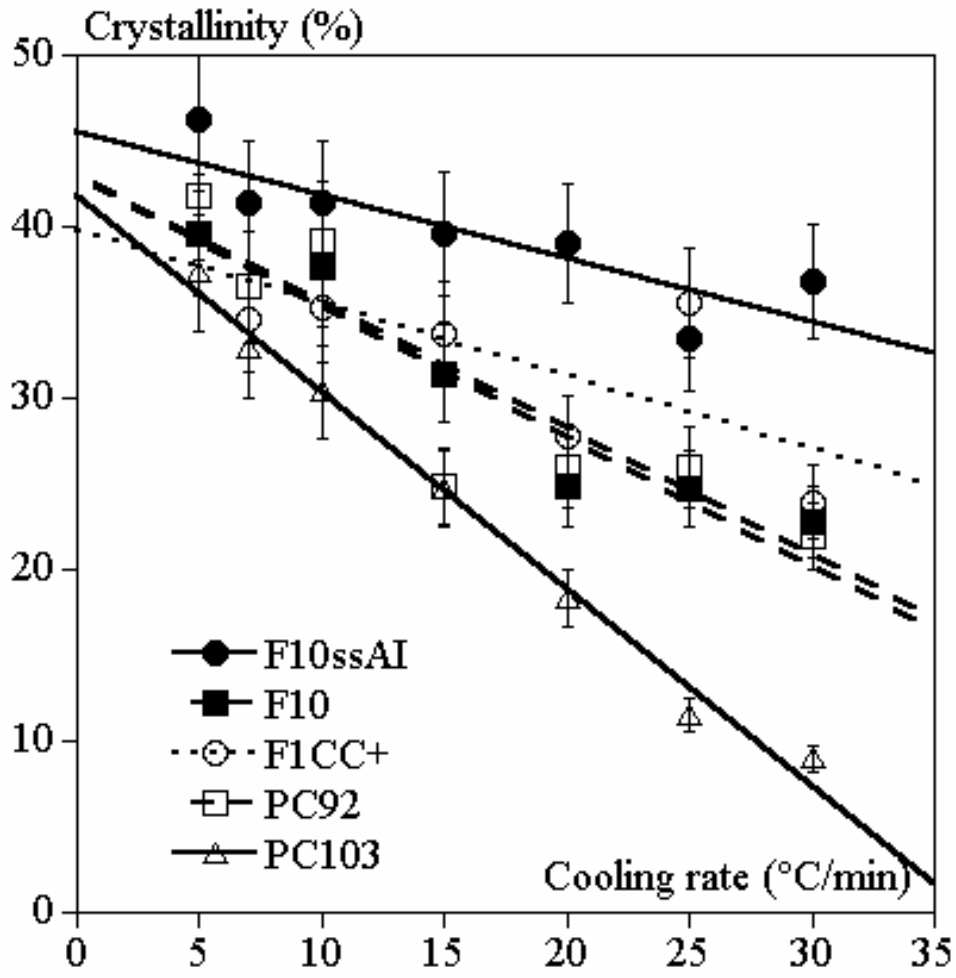
Crystallinity (%)
50
40
30
20
10
0
0
5
10
15
20
25
30
35
F10ssAI
F10
F1CC+
PC92
PC103
Cooling rate (°C/min)

Fig. 4

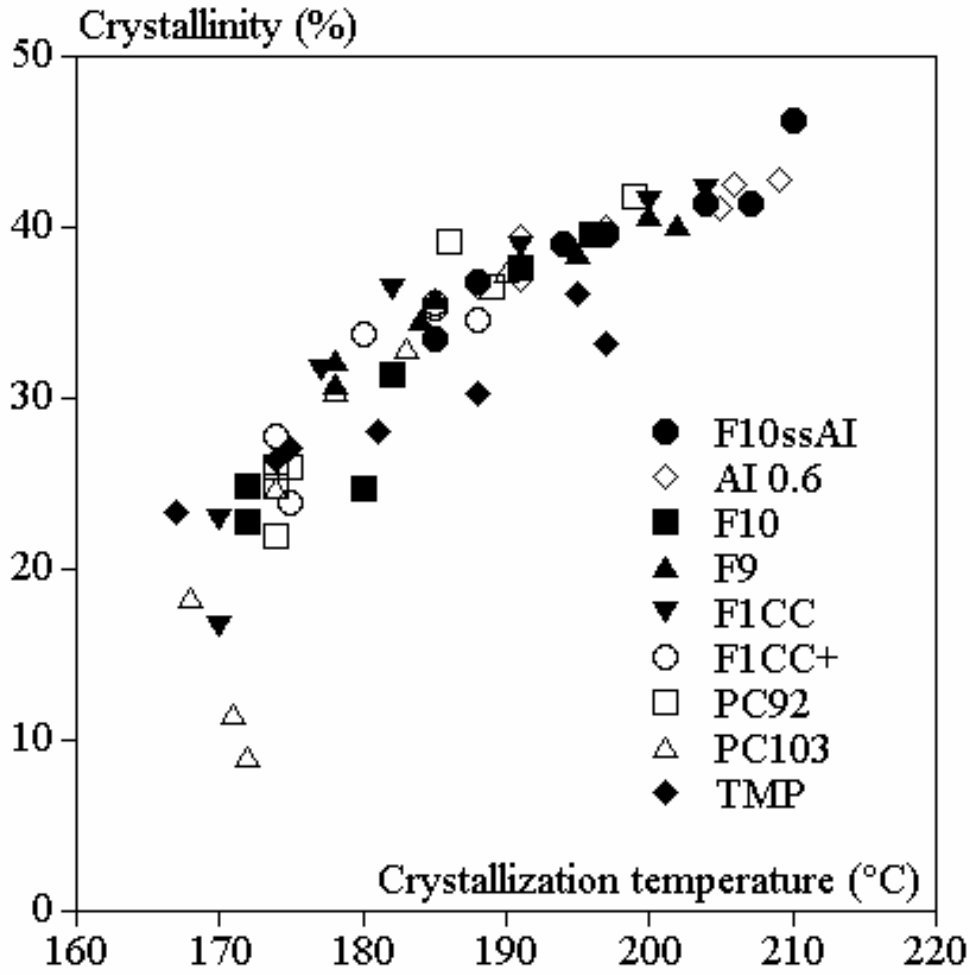
Crystallinity (%)
50
40
30
20
10
0
160
170
180
190
200
210
220
Crystallization temperature (°C)
F10ssAI
AI 0.6
F10
F9
F1CC
F1CC+
PC92
PC103
TMP

Fig. 5

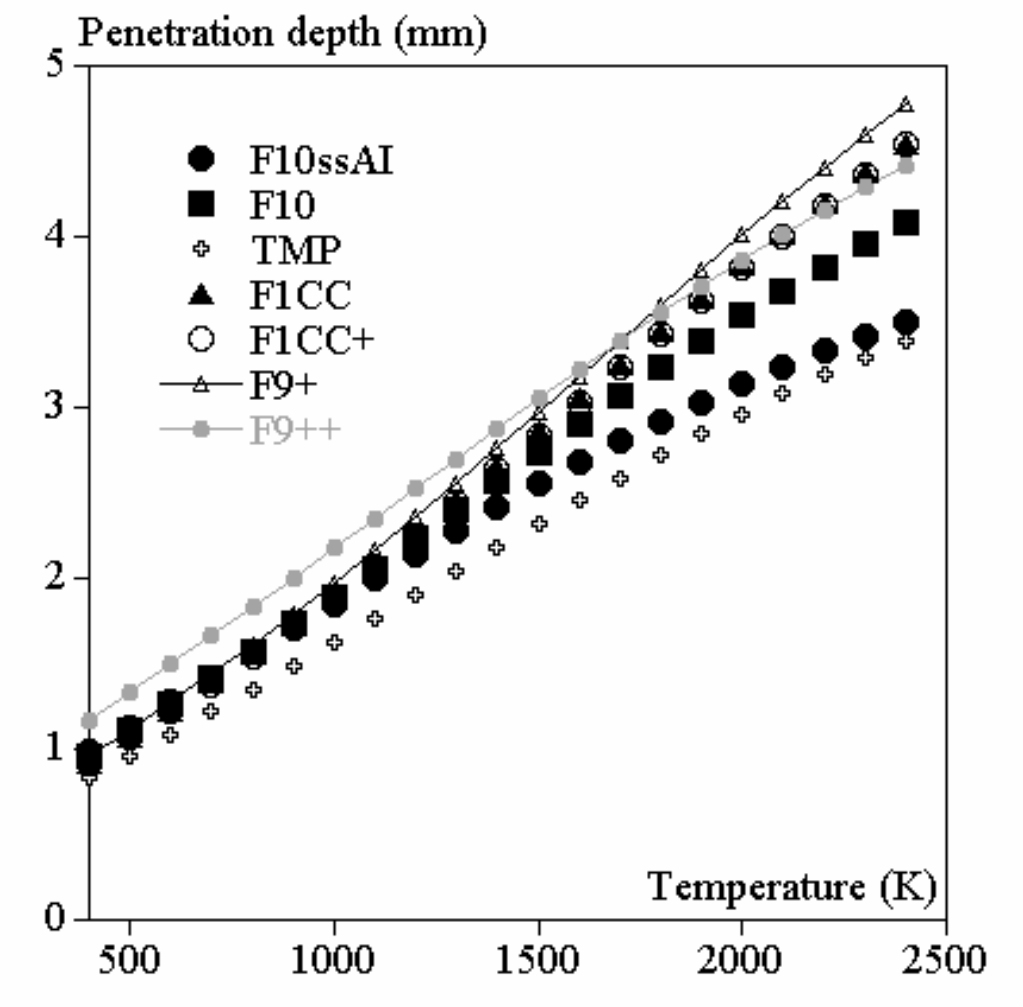
Penetration depth (mm)
5
4
3
2
1
0
F10ssAI
F10
TMP
F1CC
F1CC+
F9+
F9++
Temperature (K)
500
1000
1500
2000
2500

Fig. 6

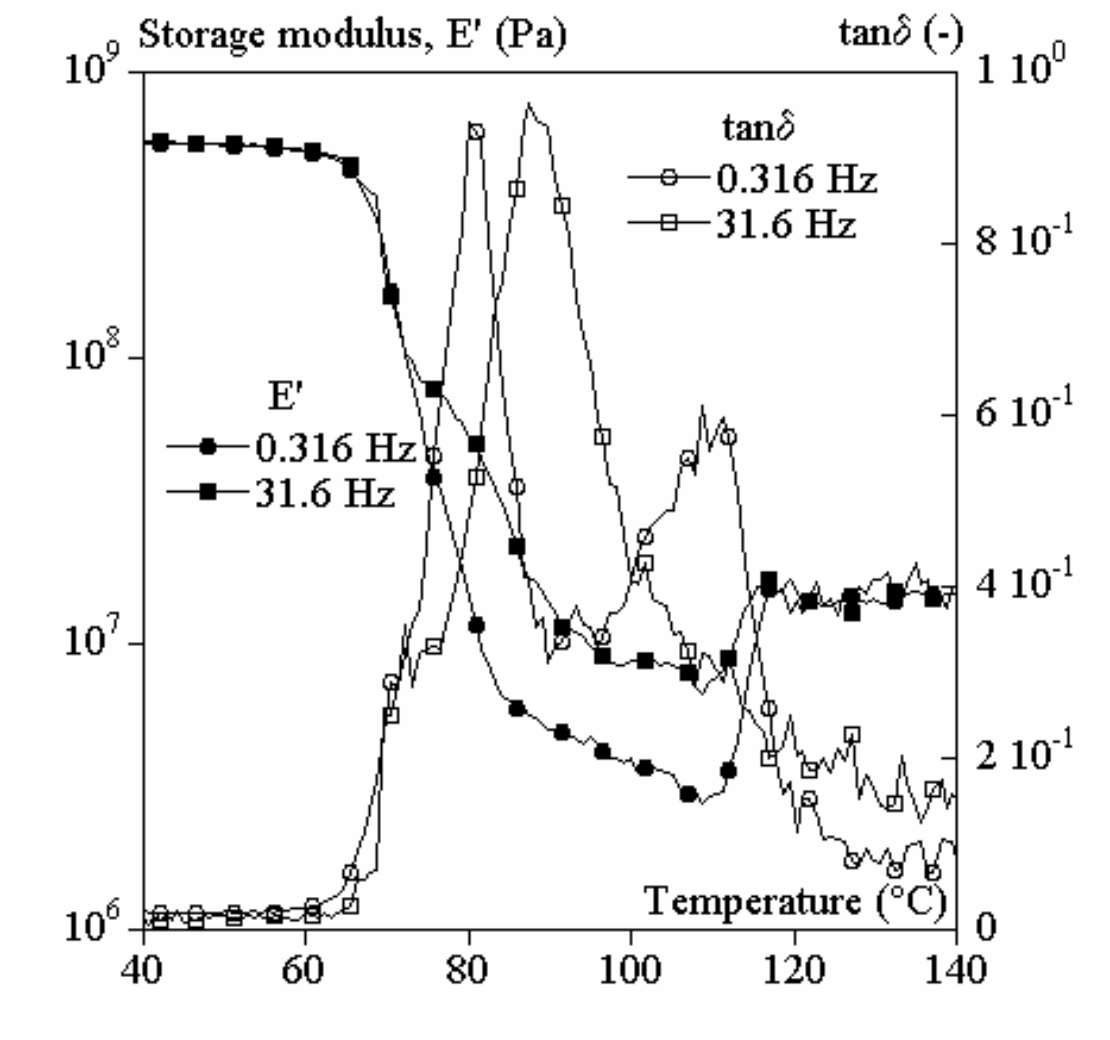
Storage modulus, E' (Pa)
tanδ (-)
10^9
10^8
10^7
10^6
1 10^0
8 10^-1
6 10^-1
4 10^-1
2 10^-1
0
tanδ
0.316 Hz
31.6 Hz
E'
0.316 Hz
31.6 Hz
Temperature (°C)
40
60
80
100
120
140

Fig. 7

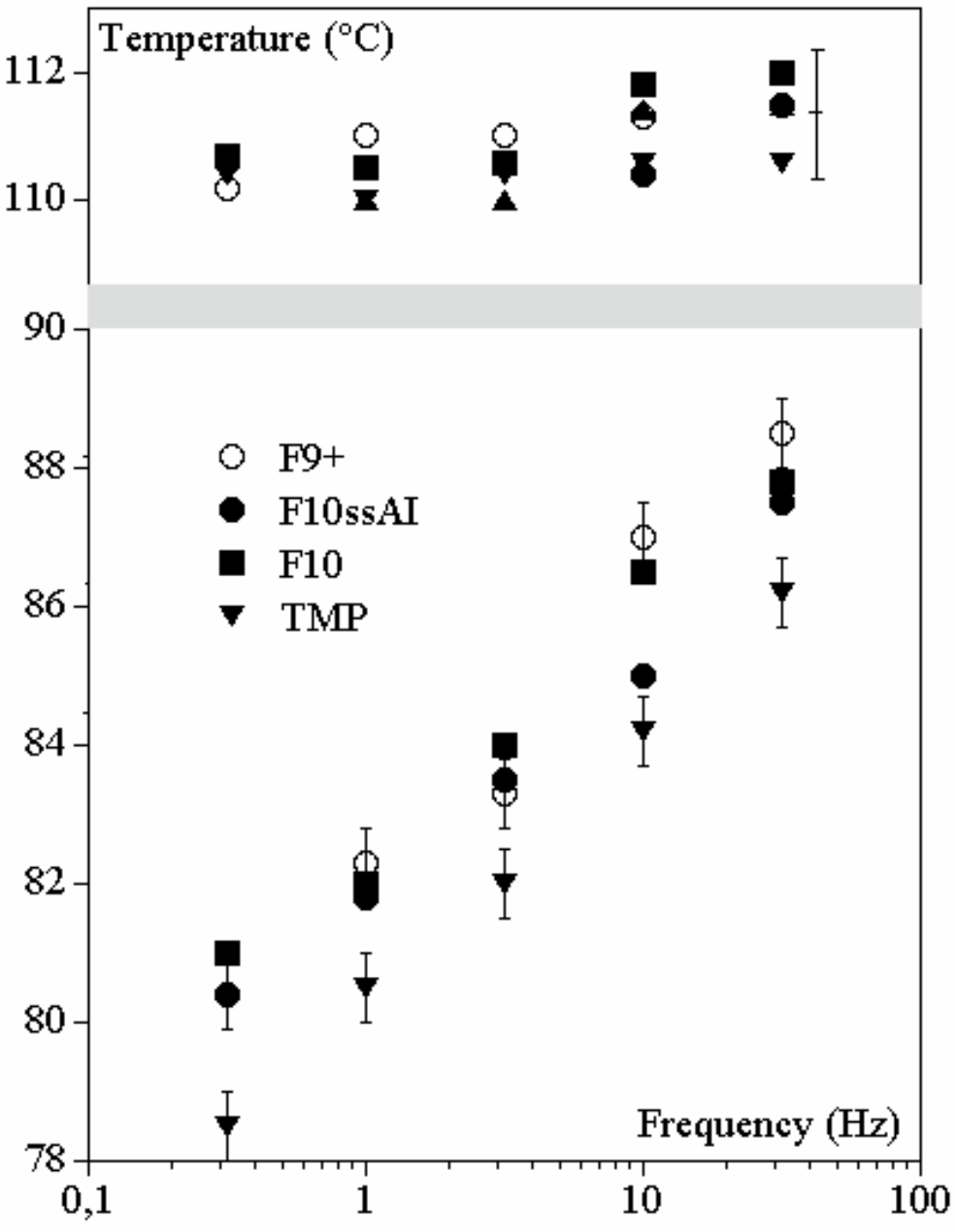
Temperature (°C)
112
110
90
88
86
84
82
80
78
F9+
F10ssAI
F10
TMP
Frequency (Hz)
0,1
1
10
100

Fig. 8

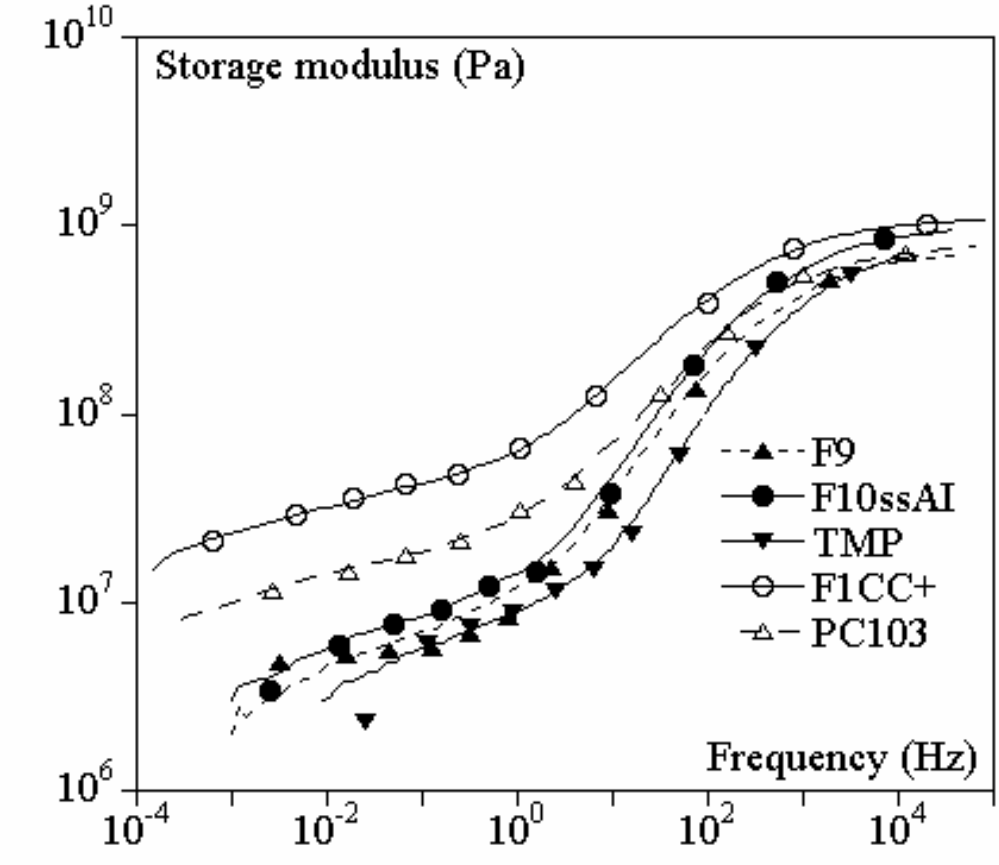
Storage modulus (Pa)
10^{10}
10^{9}
10^{8}
10^{7}
10^{6}
10^{-4}
10^{-2}
10^{0}
10^{2}
10^{4}
Frequency (Hz)
F9
F10ssAI
TMP
F1CC+
PC103

Fig. 9

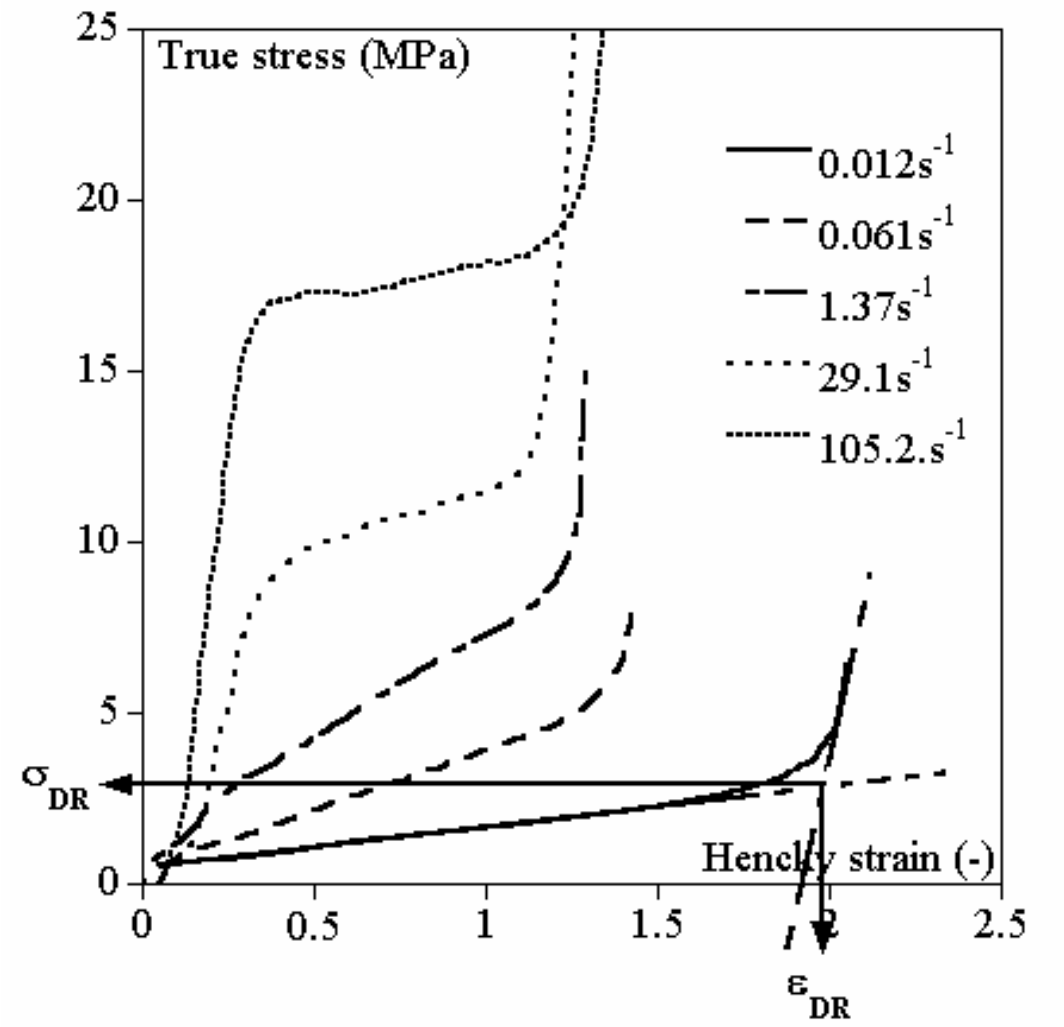
True stress (MPa)
0.012s-1
0.061s-1
1.37s-1
29.1s-1
105.2.s-1
σDR
εDR
Hencky strain (-)
25
20
15
10
5
0
0
0.5
1
1.5
2
2.5

Fig. 10

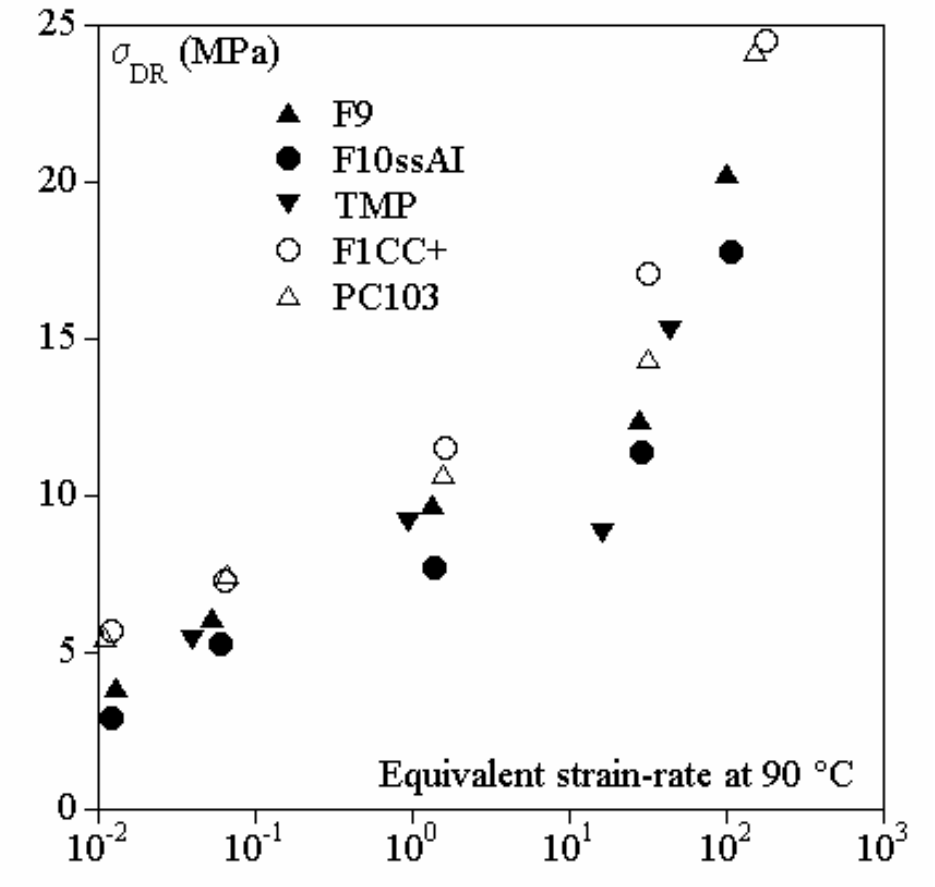

Fig. 11A

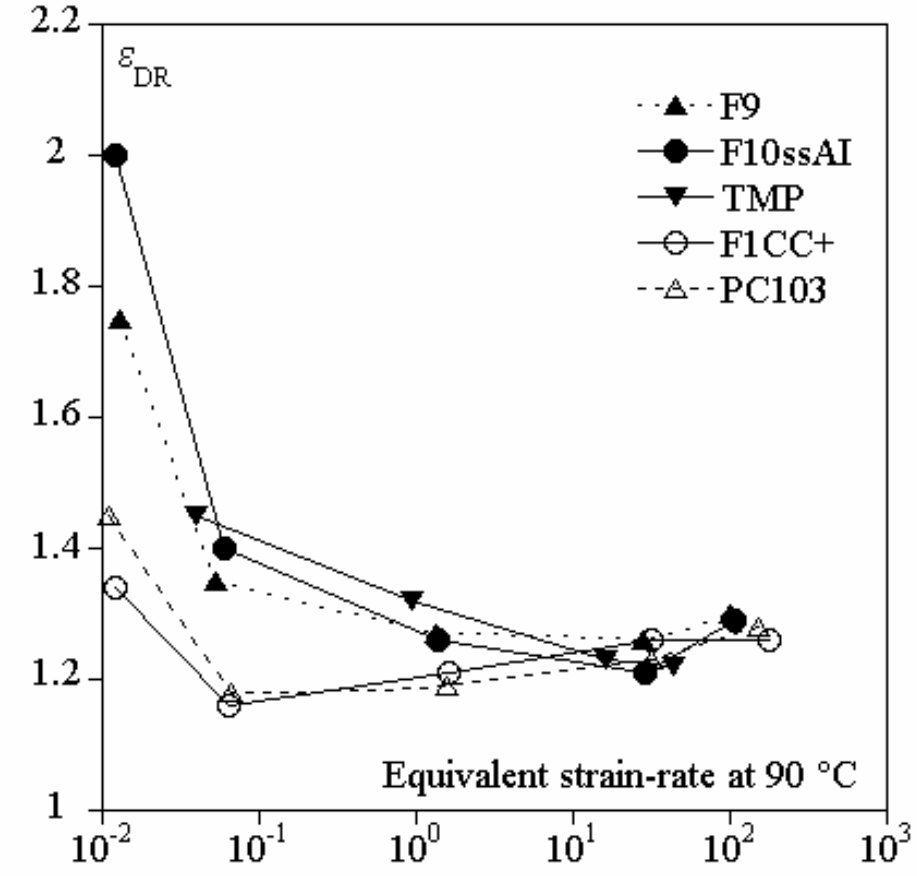

Fig. 11B

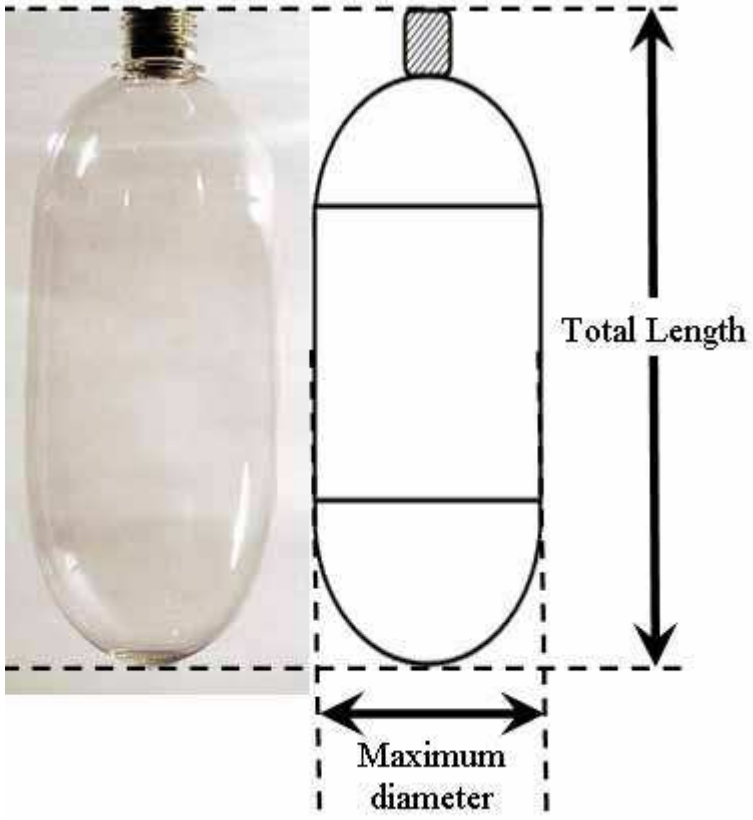

Fig 12

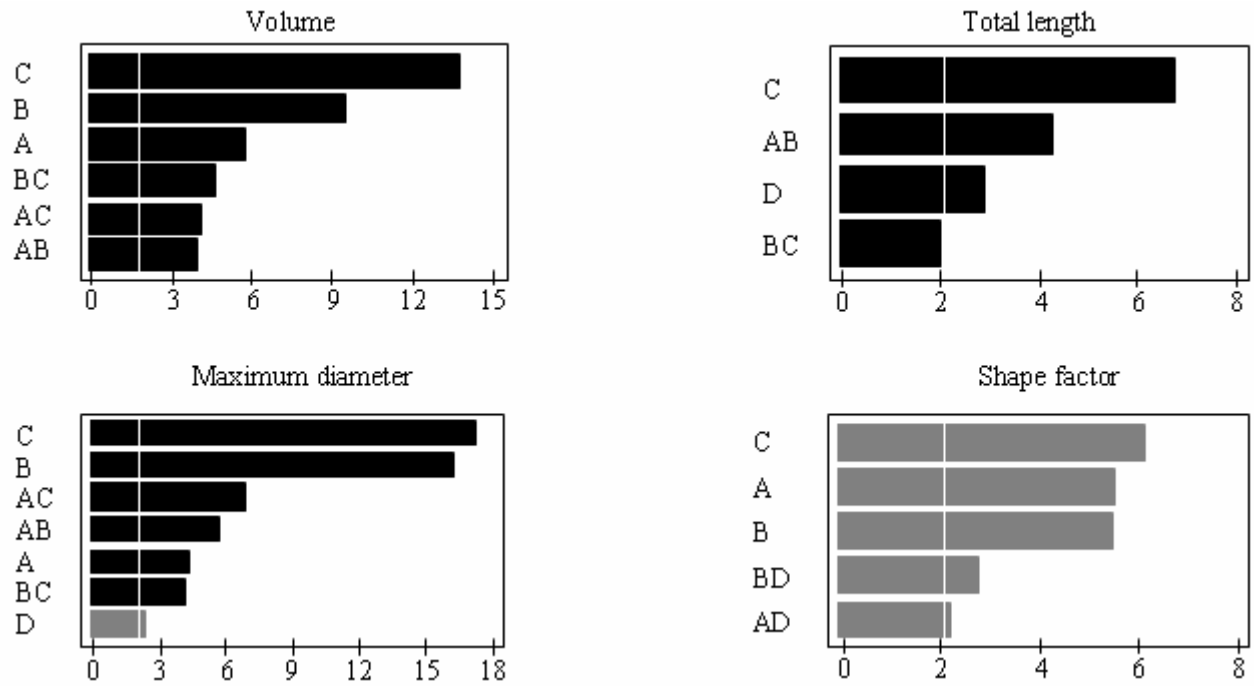
Volume
C
B
A
BC
AC
AB
0
3
6
9
12
15
Total length
C
AB
D
BC
0
2
4
6
8
Maximum diameter
C
B
AC
AB
A
BC
D
0
3
6
9
12
15
18
Shape factor
C
A
B
BD
AD
0
2
4
6
8

Fig. 13

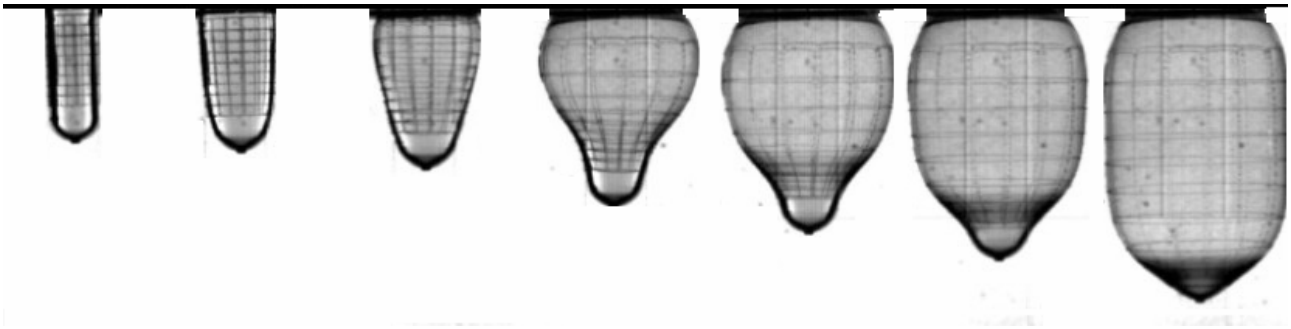

Fig. 14

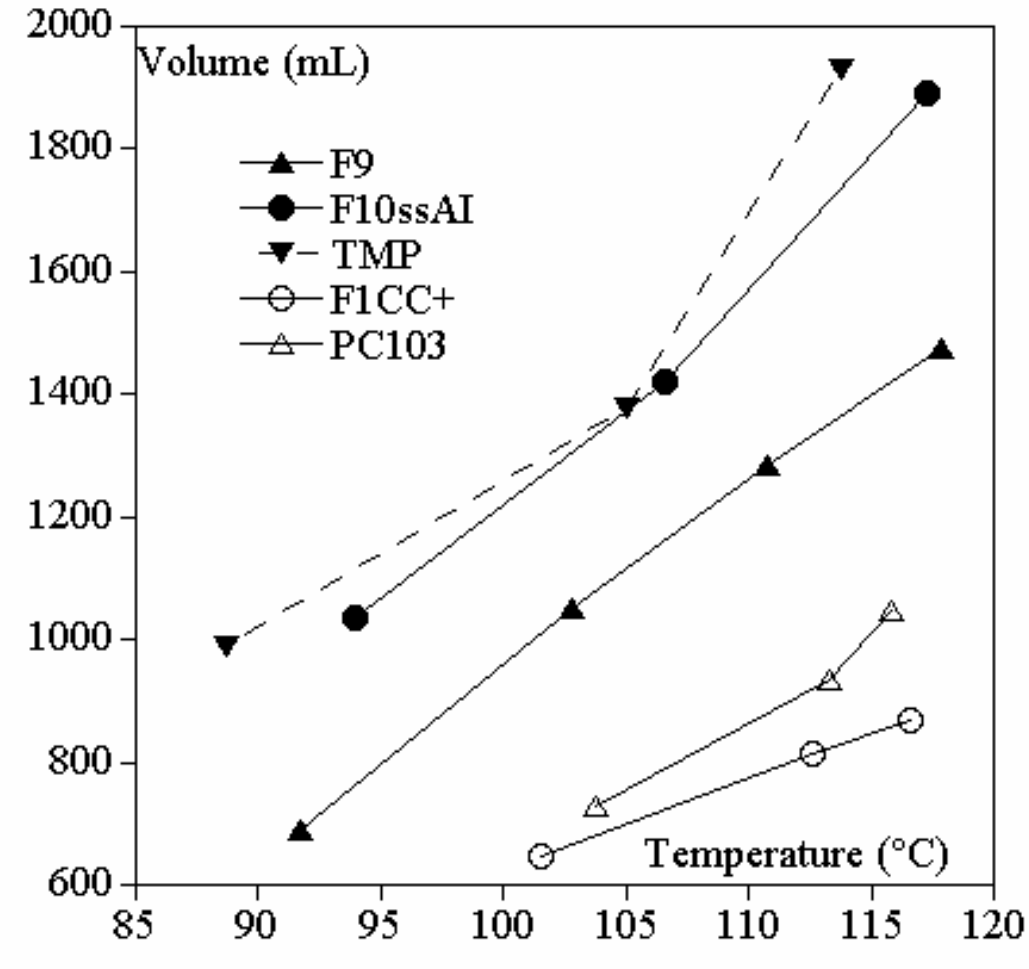
Volume (mL)
F9
F10ssAI
TMP
F1CC+
PC103
Temperature (°C)
2000
1800
1600
1400
1200
1000
800
600
85
90
95
100
105
110
115
120

Fig. 15

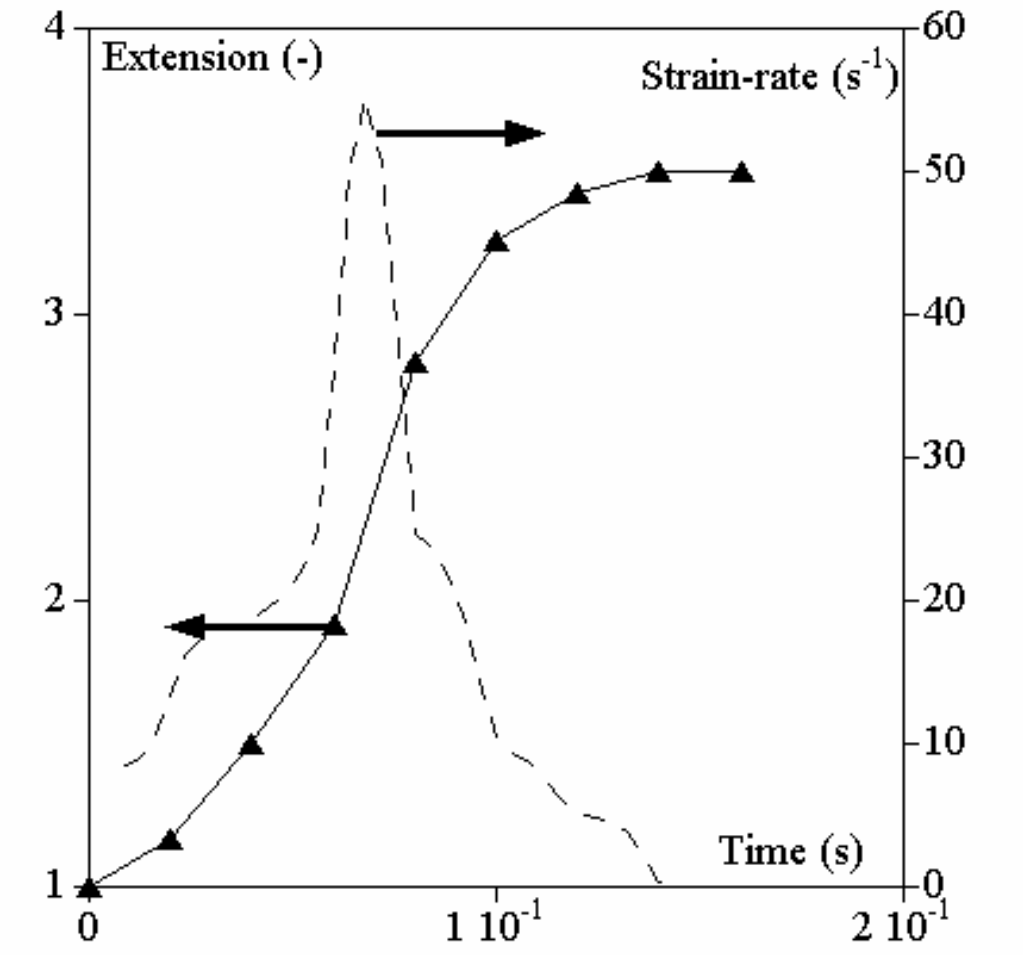
Extension (-)
Strain-rate (s^{-1})
Time (s)
4
3
2
1
60
50
40
30
20
10
0
0
1 10^{-1}
2 10^{-1}

Fig. 16

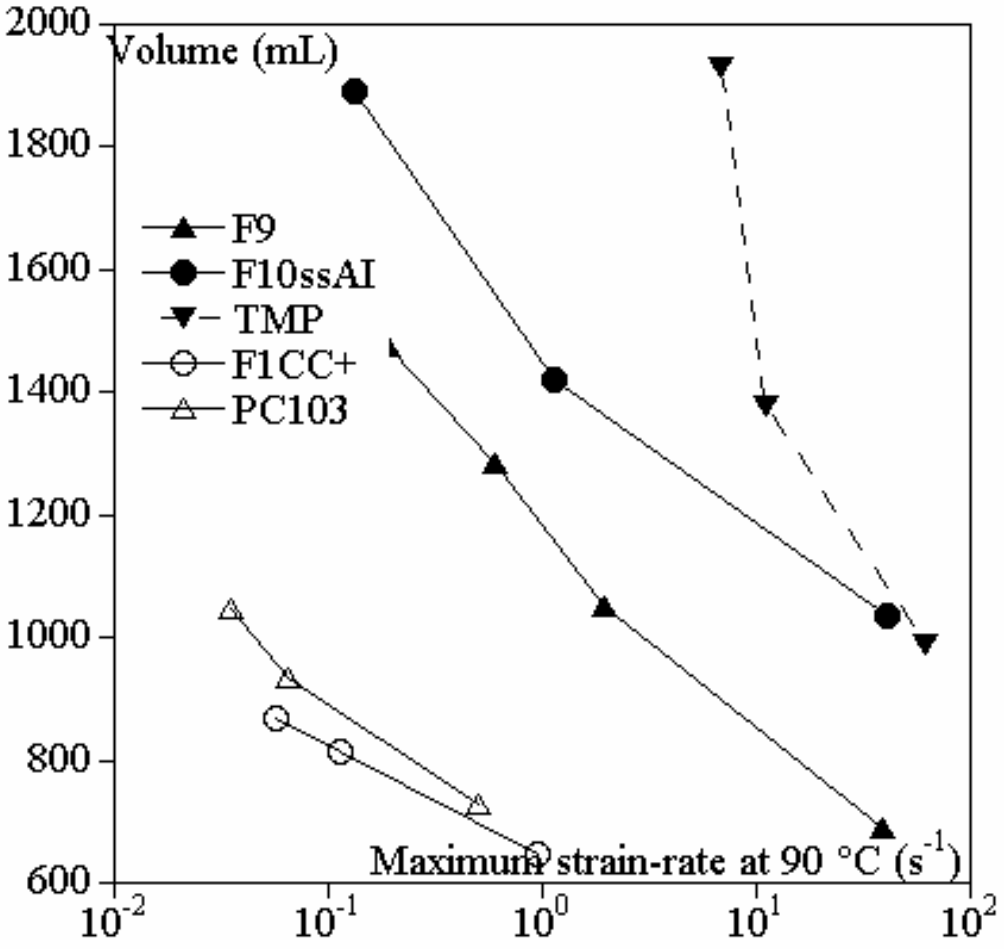
Volume (mL)
2000
1800
1600
1400
1200
1000
800
600
F9
F10ssAI
TMP
F1CC+
PC103
Maximum strain-rate at 90 °C (s-1)
10-2
10-1
100
101
102

Fig. 17

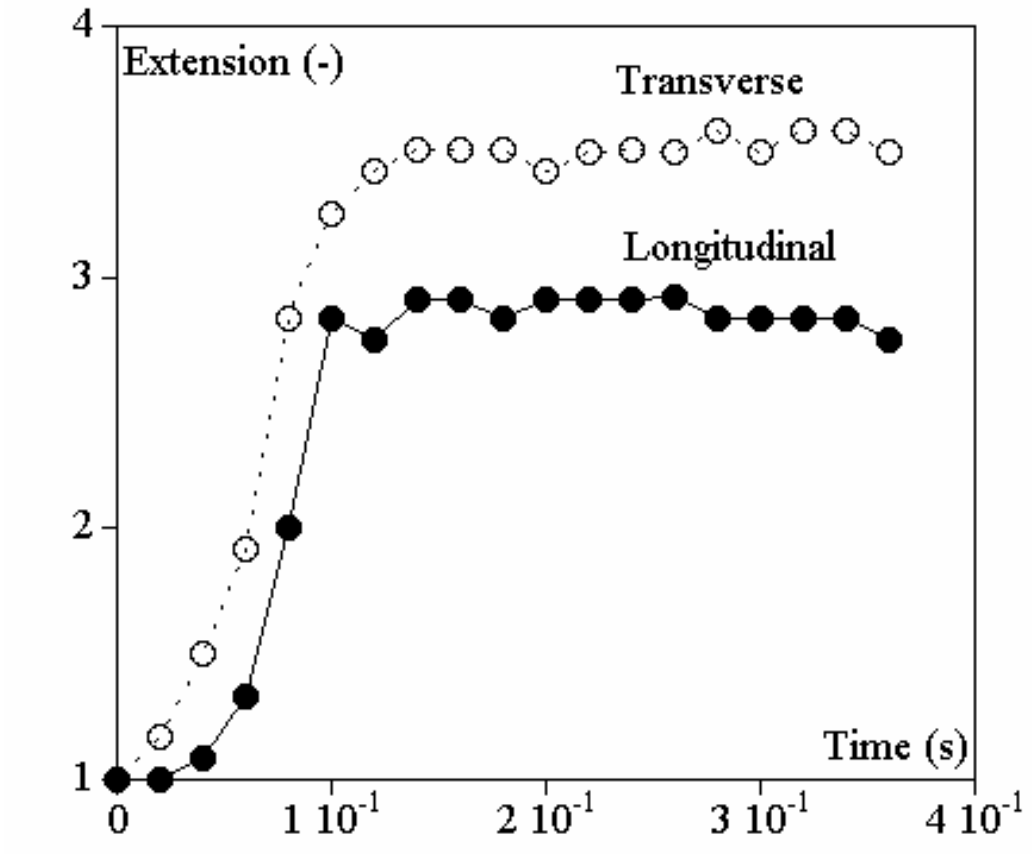
Extension (-)
Transverse
Longitudinal
Time (s)
4
3
2
1
0
1 10-1
2 10-1
3 10-1
4 10-1

Fig. 18

::

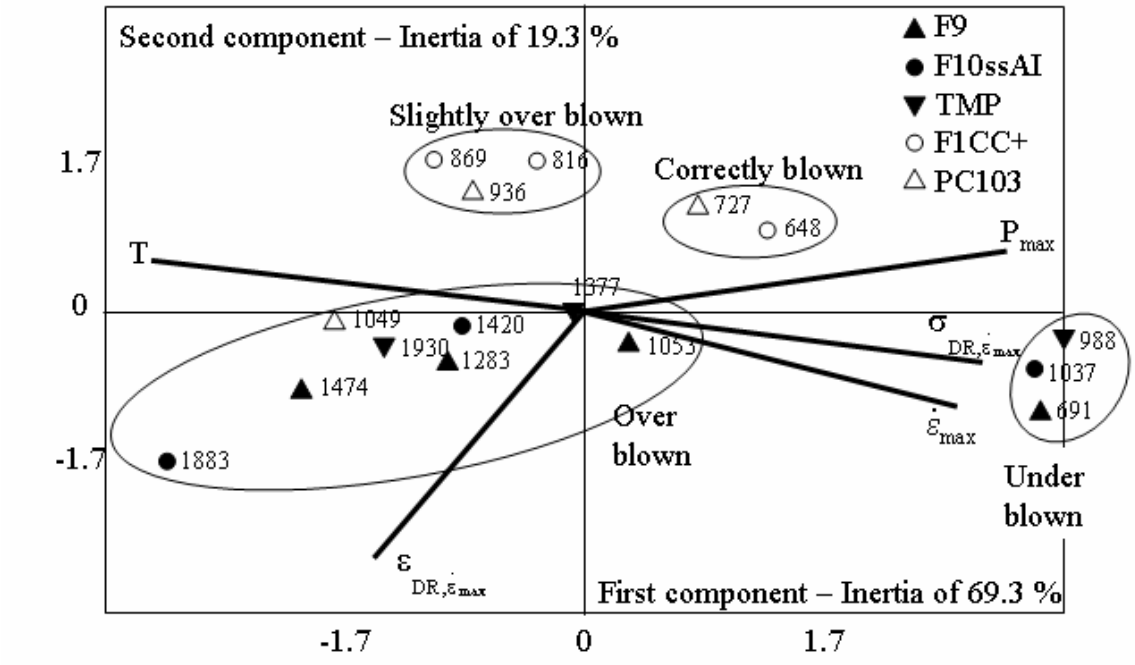
Second component – Inertia of 19.3 %
F9
F10ssAI
TMP
F1CC+
PC103
Slightly over blown
869
816
936
Correctly blown
727
648
1.7
T
P_{max}
0
1377
1049
1420
1930
1283
1053
1474
$\sigma_{DR,\dot{\varepsilon}_{max}}$
988
1037
691
$\dot{\varepsilon}_{max}$
Over
blown
-1.7
1883
Under
blown
$\varepsilon_{DR,\dot{\varepsilon}_{max}}$
First component – Inertia of 69.3 %
-1.7
0
1.7

Fig. 19

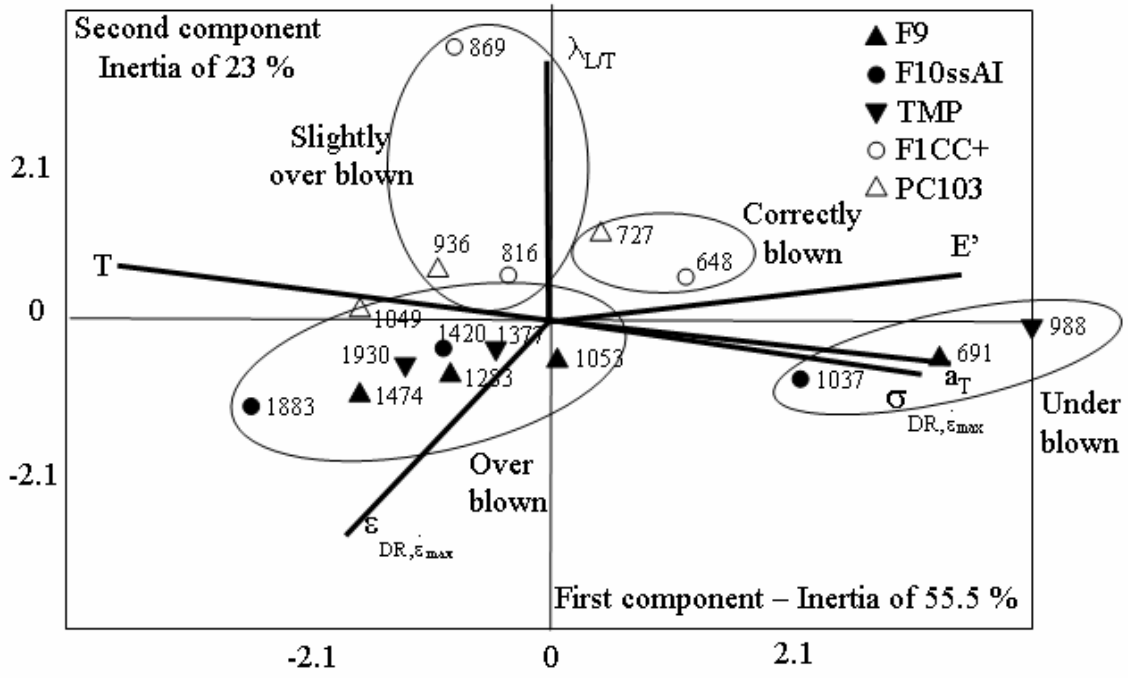
Second component
Inertia of 23 %
2.1
0
-2.1
Slightly
over blown
869
λL/T
F9
F10ssAI
TMP
F1CC+
PC103
Correctly
blown
E'
727
648
936
816
T
1049
1420
1377
1930
1053
988
691
1037
aT
σ
DR,εmax
1883
1474
1283
Under
blown
Over
blown
ε
DR,εmax
First component – Inertia of 55.5 %
-2.1
0
2.1

Fig. 20

Ref.	DEG (% mol.)	IPA (% mol.)	TMP (% mol.)	VI/IV (10mL/g)/(dL/g)	Sb (ppm)	AA (ppm)	TAG (eq H^+)
F10ssAI	2.2	0.2	0	707/0.63	248	29	42
AI0.6	2.2	0.7	0	701/0.62	280	36	41
F10	2.2	2.2	0	724/0.64	284	0.9	58
F9	2.0	2.1	0	844/0.74	281	0.7	42
F9+	2.6	2.3	0	1006/0.85	266	0.4	31
F9++	2.4	2.3	0	1166/0.97	-	0.4	-
F1CC	1.7	0	0	723/0.64	164	80	29
F1CC+	1.3	0	0	1030/0.87	200	0.7	19
PC92	1.5	0	0	924/0.79	196	0.9	21
PC103	1.3	0	0	950/0.81	198	0.9	20
TMP	3.9	2.4	0.4	834/0.73	195	>50	21

Table 1

	95°C	85°C			80°C
	0.5 $mm.s^{-1}$		10 $mm.s^{-1}$	150 $mm.s^{-1}$	
F9	0.013	0.053	1.34	28.0	99.0
F10ssAI	0.012	0.061	1.37	29.1	105.2
TMP	0.018	0.040	0.94	16.3	43.1
F1CC+	0.012	0.065	1.60	31.2	180.5
PC103	0.011	0.067	1.55	31.7	153.9

Table 2

Heating profile from top to bottom of the preform :	
Lamp L1 Lamp L2 Lamp L3 Lamp L4 Lamp L5	75% 55% 45% 65% 60%
General power (Average temperature of the preform)	75% (107°C)
Pressure	0.7 MPa (7 bar)
Low-blow duration	200 ms
Rod length (Effective stretching length)	0.13 m (0.113 m)
Low-blow delay in term of percentage of stretching length (Stretching length, location index)	9.4% (0.011 m, 26)

Table 3

Parameter	Minimum	Maximum
A General power (%)	65	80
B Pressure (MPa)	0.5	0.7
C Low-blow duration (ms)	100	400
D Rod length (m)	0.10	0.13
E Low-blow delay end (Location index)	26	28

Table 4